DESIGN OF A LASER-BASED PROFILE MONITOR FOR LINAC4 COMMISSIONING AT 50 MeV AND 100 MeV

T. Hofmann*, E. Bravin, U. Raich, F. Roncarolo, CERN, Geneva, Switzerland
S. Gibson, A. Bosco, G. Boorman
John Adams Institute at Royal Holloway, University of London, Egham, United Kingdom
E. Griesmayer, CIVIDEC Instrumentation, Vienna

Abstract

A laser-based profile monitor has been designed for commissioning of CERN's LINAC4 accelerator at 50 MeV and 100 MeV, as part of the development of a non-destructive profile and emittance monitor foreseen for the final 160 MeV beam. The system is based on a low power laser which is scanned through the H^- beam. Electrons, which are photo-detached from the ions by the laser, are deflected by a steerer magnet and measured by a diamond detector. The custom designed diamond detector is tailored to minimize the disturbance due to the electromagnetic field of the passing main beam. The laser source will be installed in the LINAC4 Klystron gallery located 75 m away from the profile station and an optical fiber will transport the laser to the tunnel. The laser propagation for different pulse length and peak power values was characterized with laboratory tests with such a long fiber. In this paper we describe the overall design, focusing on key elements such as the fiber-based laser transport and the electron detection with the diamond detector.

INTRODUCTION

As the LINAC4 construction advances, its commissioning is taking place in stages at different beam energies, as indicated in Fig. 1. So far, all the accelerator's equipment and the beam parameters have been validated up to the exit of the first DTL tank (12 MeV).

The conventional techniques which are foreseen to measure the beam profile and transverse emittance, like SEM-grids or wire-scanners, are all destructive or at least invasive with respect to the ion beam.

During the 3 MeV and 12 MeV commissioning, a non-invasive laser system was successfully operated to measure the vertical emittance of the H^- beam, by collecting the neutralized H^0 atoms [1–3].

The next two stages of the LINAC4 commissioning will be used to check the performance of a modified version of the laser-based instrument. The system will be part of a diagnostics test bench that will be temporarily installed after the last DTL cavity (50 MeV) and then moved after last CCDTL cavity (100 MeV).

For these development stages, the system will be setup for measurements in the vertical plane only, with the aim of demonstrating the ion beam profile reconstruction by collecting the electrons that are photo-detached during the laser scan [4].

* thomas.hofmann@cern.ch

The main novelty of our system with respect to those in other facilities [5,6] will be the use of a relatively low power laser and of a fast diamond detector as electron collector.

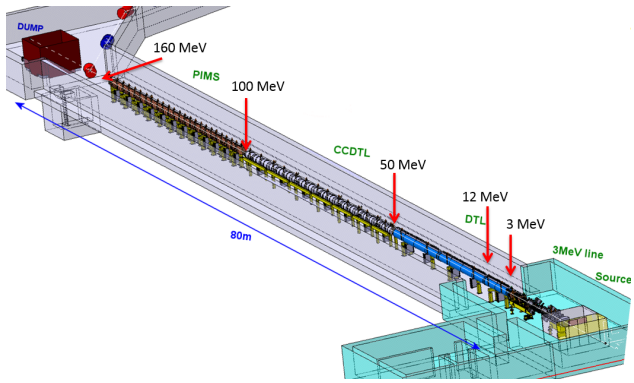

Figure 1: LINAC4 facility indicating the beam energy that will be reached during the different commissioning stages. The laser stripping system has already been tested at 3 MeV and 12 MeV periods and is presently setup for 50 MeV and 100 MeV before being permanently installed at 160 MeV.

CONCEPTUAL DESIGN

The conceptual and mechanical design of the system is shown in Fig. 2. Since in our application the laser beam is relatively small with respect to the H^- beam size, the vertical position of the liberated electrons is well defined and counting the stripped electrons as function of the laser position during a scan allows the beam profile to be reconstructed. A dipole magnet located just after the laser interaction point (IP) is used to extract the electrons toward the diamond detector designed to integrate the electron signal. Due to the much lower energy of the stripped electrons with respect to the H^- ions, the magnetic field necessary to extract the electrons has a very weak effect on the main beam.

As the detachment cross section is small and during a linac pulse only a tiny H^- beamlet is traversed by the laser, less than 10^8 H^- ions per linac pulse are neutralized (i.e. lost). Compared with the total pulse charge of 10^{14} for the nominal beam current (40 mA), this technique can therefore be considered as non-invasive.

LASER DELIVERY, TRANSPORT AND FOCUSING

The selected fiber-laser (V-Gen VPFL-ISP-1-40-50) operates at a wavelength of 1064 nm, with kilowatt peak powers

ISBN 978-3-95450-176-2

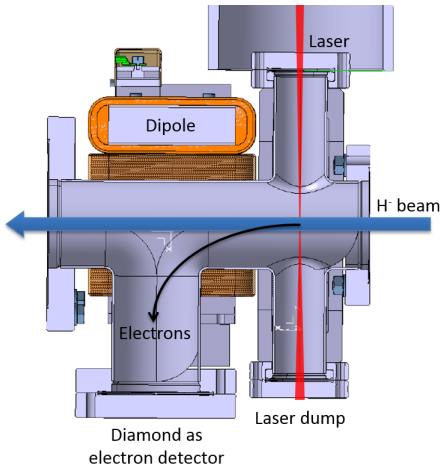

Figure 2: Conceptual design of the laser profile monitor.

and pulse-lengths variable from 1 ns to 300 ns. This is significantly different from existing systems [6, 7], based on q-switched Nd-YAG lasers with peak powers 3 orders of magnitude higher.

The low peak-power facilitates the laser operation/safety measures and allows the laser to be transported from its location in the klystron gallery to the interaction point (IP) by means of a large-mode-area (LMA) optical fiber [8]. This represents a distance of 20 m to the final position at 160 MeV and 75 m to the 50 MeV area (see Fig. 1). This technique greatly reduces the complexity of the transport system and thus provides a reliable solution with minimal maintenance. The remaining challenges are the high power densities at the end-facets [9] and non-linear effects in the fiber, which limits the transmitted peak power [10].

The optical setup to focus the laser to the IP consists of collimation and focusing optics which are mounted on a vertical stage to scan the laser across the H^- beam. Furthermore an optical path to characterise the laser pulse shape and M^2 is added. More details can be found in [1].

75 m Fiber Transmission

Looking into theory, Stimulated Brillouin Scattering (SBS) is the dominant non-linear effect, limiting the transmission through the fiber. This effect increases with the length of the fiber and acts above a certain peak power threshold, causing Stokes-shifted back-reflections due to spontaneous light scattering at thermal phonons. The threshold peak power is defined in [10] as,

$$P_{B,th} = C_{B,th} \frac{1}{\gamma_B L_{eff}} \qquad (1)$$

where $C_{B,th}$ is the critical factor, γ_B is the fiber-specific Brillouin coefficient and L_{eff} the fiber length. Moreover, SBS also depends on the spectral width of the stimulating laser pulse. For shorter pulses corresponding to wider spectra the effect is less dominant. As $C_{B,th}$ and γ_B is not known for the LMA fiber, a test in the laboratory was performed to characterize the laser transmission

Figure 3 shows the pulse shape before and after the fiber transmission for different pulse energies. The pulses after transmission are clearly delayed by 375 ns, which corresponds to the light propagation along 75 m. Distortions in pulse shape and pulse width cannot be observed even for peak powers above 2 kW.

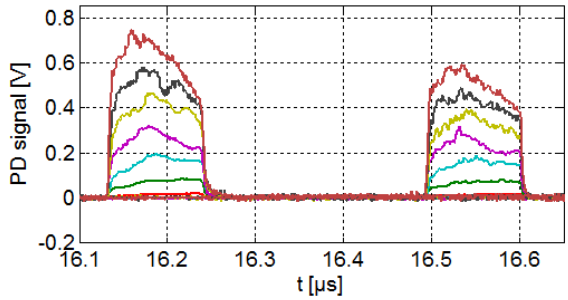

Figure 3: Laser pulses with different energies before (left) and after fiber (right).

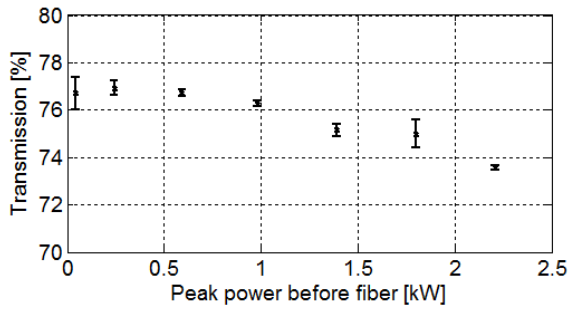

Figure 4: Laser transmission through the 75m large-mode-area (LMA) optical fiber.

By using an energy meter with a large surface detector, the overall transmission of the laser pulses could also be measured for different peak powers. The plot in Fig. 4 shows a transmission above 75% below 1 kW peak power and slightly lower transmission for higher pulse peak powers. The tests were not continued beyond the 2 kW level, in order not to damage the fiber end-facets before the actual beam measurements. The experiences gained during the measurement campaigns at 3 MeV and 12 MeV [1, 2] makes us confident that sufficient electron stripping can be achieved with laser peak powers below 1 kW. Measurements with 5 ns, 10 ns and 30 ns pulse lengths confirmed the high transmission for similar high peak powers.

After these laboratory tests we concluded that the fiber transmission with peak powers below 2 kW works very reliably and is not significantly affected by SBS.

Another challenge for kilowatt fiber transmission is the coupling into the fiber core. The LMA-fiber we are using has a 20 µm core diameter, which can lead to power densities of more than 100 J/cm^2. In this regime ablation can take place and damage the end-facet [9].

To handle this problem, fiber connectors with inserted end-caps were chosen. As illustrated in Fig. 5, the core material is expanded into the cladding area. In this way,

ISBN 978-3-95450-176-2

the laser must be focused inside the fiber to maximise the transmission, which means that the power density at the fiber surface is greatly reduced.

Using this technique no issues with burned end-facets were observed, in contrast to what occurred during the measurements with the LINAC4 3 MeV beam, when the fiber was not equipped with end-cap connectors.

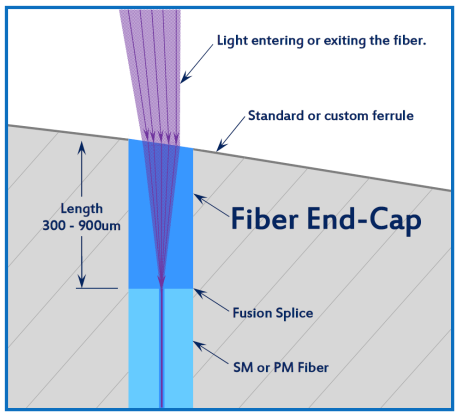

Figure 5: Principle of end-cap fiber facet [11].

ELECTRON MONITORING

As shown in Fig. 2, the dipole magnetic field guides the detached electrons from the main H^- beam axis into a T-shaped vacuum chamber hosting the diamond detector. In this section the magnet and detector design will be described.

Electron Deflector

The electrons kinetic energy is only 27 keV, as can be derived from the 50 MeV H^- energy and the proton to electron mass ratio. These low energy electrons can be deflected by 90° with an integrated field of only 0.9 mTm.

Steerer magnets used routinely at LINAC4 can provide up to 3.5 mTm integrated field. We therefore decided to modify one of these steerer magnets as a simple and cost-effective solution. By removing the magnet coil on the T-chamber side, the steerer acts as a C-shaped magnet with the remaining coil powered to create the field.

To predict the electron trajectories in the modified steerer field, a magnetic field-map was created. In Fig. 6 the B-field in the Y-plane is plotted. The trajectories for the stripped electrons were simulated using as input the beam dynamics data in the plane of the laser interaction (X = 0 mm; Z = -83 mm) and the magnetic vector-field. In addition to the Lorentz force, space charge effects of the main H^- beam and synchrotron radiation was taken into account but had no significant effects on the paths of the electrons.

In Fig. 6 the black curve represents the 3-sigma envelope of the electron trajectory when powering the magnet coil with a current of 4.7 A. The dark blue bar at Z = -60 mm represents a shielding which surrounds the beam-pipe between laser IP and steerer magnet. The shielding outside the vacuum chamber was designed to modify the magnetic field lines in order to avoid electrons being deflected too early after the stripping process and subsequently hitting the wall of the beam-pipe before reaching the extraction channel towards the electron monitor.

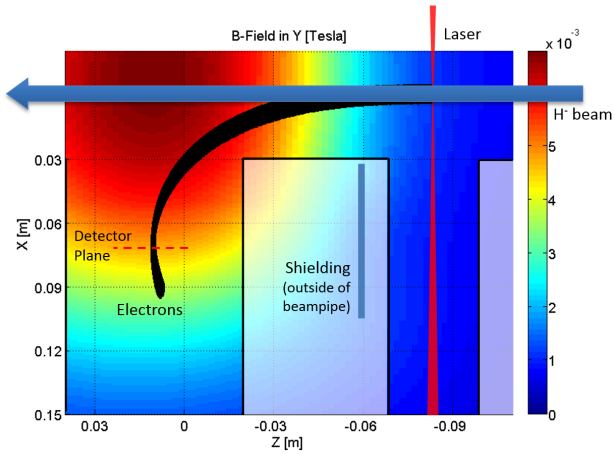

Figure 6: Magnetic field map (in Tesla) and electron trajectories (black) from the laser interaction point to the diamond detector. White areas are outside of beam-pipe.

Figure 7 visualizes an overlay of electron distributions, generated during the laser scanning process, arriving at X = 72 mm. It represents the superposition of the stripped electrons at each laser position during the vertical laser-scan. For one laser position, the width of the distribution in the Y-plane would be less than 1 mm. The detector position X = 72 mm was chosen, as this is the focal point generated by the weak focusing of the dipole.

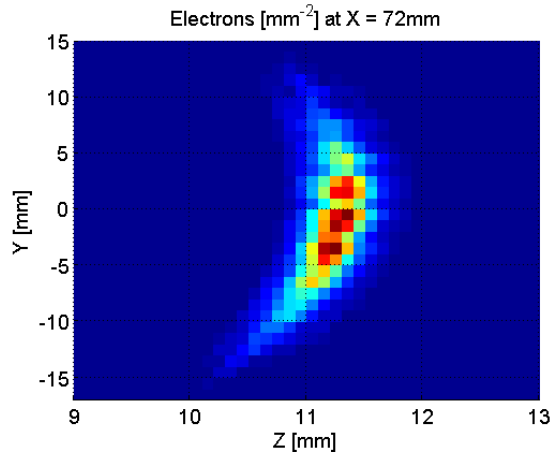

Figure 7: Expected electrons distribution at the detector plane, accounting for all laser positions during a scan.

Diamond Detector

A laser pulse with 100 µJ pulse-energy and 100 ns pulse-length is expected to detach approx. $5 \cdot 10^5$ electrons from the atomic cores. The detection of such a small number of low energy electrons (E_{kin} =27 keV) required the design

ISBN 978-3-95450-176-2

of a high sensitivity and fast (to cope with the short laser pulses) detector.

After considering various options, it was decided to design and fabricate a single-crystal chemical vapor deposition (sCVD) diamond detector, capable of providing a fast response, high sensitivity and radiation hardness. A picture of the detector that was recently installed in the laser profile meter tank assembly is shown in Fig. 8.

The front electrode of the detector facing the electron beamlet is bonded to ground potential all around its perimeter to avoid electro-magnetic disturbance from the main H^- beam passing just 72 mm away from the detector.

Due to the low range of the electrons (6 µm in diamond) this front electrode must be as thin as possible in order to minimize energy loss. Table 1 lists the front electrode layer materials and associated energy loss. In summary, 3.2 keV of the electron's energy is absorbed in the electrode layers while 23.8 keV is left to create a signal in the diamond bulk.

Table 1: Diamond Detector Layer Composition

Layer	Thickness	Energy Loss of e^-
Gold	250 nm	2.3 keV
Platin	120 nm	0.7 keV
Titan	100 nm	0.2 keV
Diamond	500 µm	23.8 keV

The electron signal generation and read out is sketched in Fig. 9. The 23.8 keV energy deposition creates electron hole pairs, each requiring 13 eV (diamond's generation energy). This means that a charge of $1.5 \cdot 10^{-10}$ C is created for the $5 \cdot 10^{-5}$ electrons generated by each laser pulse, which can then be read out via the applied bias of 500 V. Due to the single crystal diamond material, no internal losses are expected. The charge is then amplified and converted to a voltage signal that can be digitized by a 1 GSps Analog-to-Digital-converter (ADC). A filter circuit, included in the preamplifier, was designed to separate the high-frequency signal of the laser pulses from low-frequency background (e.g. electrons from beam-gas ionization occurring in the drift space upstream the laser IP).

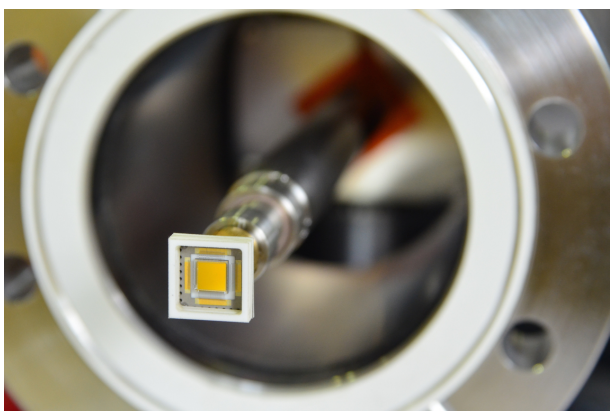

Figure 8: sCVD diamond detector [12] mounted on the actuator that is part of the laser monitor assembly for the 50 MeV experiment.

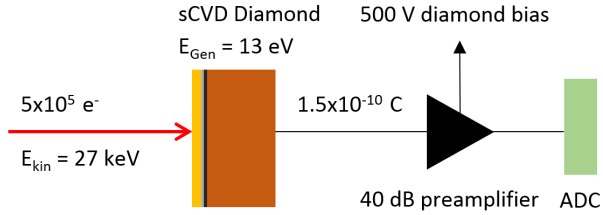

Figure 9: Signal creation and readout of the diamond detector.

In order to achieve the detector bandwidth required to resolve the laser pulses, it was decided to produce a detector with a relatively small surface (4 mm x 4 mm) to avoid parasitic capacitances. This feature also minimizes electromagnetic coupling and background due to residual gas stripping [1].

In order to ensure the collection of all electrons during a scan (see Fig. 7) with such a small detector, the diamond is mounted on an actuator that will be moved in synchronism with the laser. As the laser width is approx. 150 µm, the electron beamlet will be spread out less than one millimeter in the Y-plane of the detector. Therefore no electrons missing the diamond detector are expected.

SUMMARY AND OUTLOOK

A system for non-destructive vertical profile measurements for the LINAC4 H^- beam has been designed. The laser system consists of a pulsed laser-source, a 75 m long fiber-based laser transport line, a scanning and diagnostics assembly and a laser energy meter functioning as a laser dump. Tests of the laser delivery with a 75 m fiber have been performed and the results are very promising.

The liberated electrons will be deflected by a modified steerer magnet, with the electron trajectory optimization and the dimensioning of the detector supported by a set of dedicated electron tracking simulations accounting for space charge effects.

A sCVD diamond detector was chosen as electron collector. The monitor design was based on studies to optimize signal formation and electromagnetic shielding. It was decided to move the detector vertically synchronous with the laser to achieve a compact design with a fast response.

Figure 10 shows a picture of the system installed at LINAC4, as part of the 50/100 MeV test bench. According to the present LINAC4 schedule, first beam tests at an energy of 50 MeV are foreseen in October 2015. The next tests at 100 MeV will take place in early 2016 and will be used to gain more experience in operating the novel profile-meter to feed-in to the design of the final system. This final system will be installed permanently at the LINAC4 top energy of 160 MeV and will be designed to monitor both horizontal and vertical transverse profiles (via electron monitoring) and the transverse emittances (via H^0 monitoring).

ISBN 978-3-95450-176-2

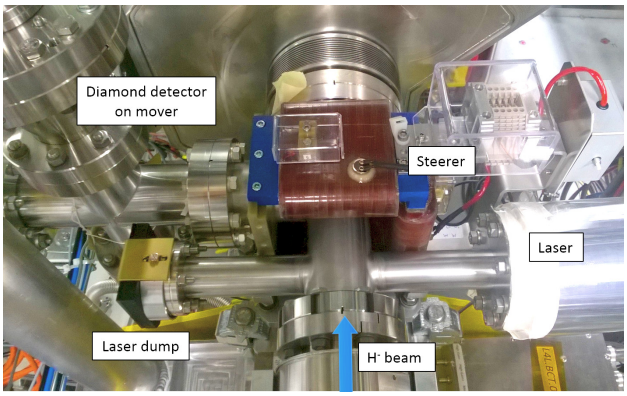

Figure 10: Installed system at the LINAC4 diagnostic test-bench.

ACKNOWLEDGEMENTS

We acknowledge the support of the Marie Curie Network LA^{3}NET which is funded by the European Commission under Grant Agreement Number GA-ITN-2011-289191.

In addition we would like to thank A. Vorozhtsov and J. Bauche for providing and commissioning of the steerer magnet and generating a magnetic field map as well as the LINAC4 commissioning team for giving us the opportunity to test our novel instrument.

REFERENCES

[1] T. Hofmann et al., “Demonstration of a Laserwire Emittance Scanner for the CERN LINAC4 H-. Beam”, to be submitted to Phys. Rev. ST, Accelerators and Beams, Preprint: arXiv:1508.05750

[2] T. Hofmann et al., “Experimental results of the laserwire emittance scanner for LINAC4 at CERN” Proceedings of Laser Applications at Accelerators Conference 2015, Mallorca, Spain

[3] S. Gibson et al., "A fibre coupled, lowpower laserwire emittance scanner at CERN LINAC4", Proceedings of IPAC2014, Dresden, Germany

[4] J.T. Broad, W.P. Reinhardt,"One- and two-electron photoejection from H^- : A multichannel J-matrix calculation", Physics Review A 14, 2159 (1976)

[5] R. Connolly et al., “A laser-wire beam-energy and beam-profile monitor at the BNL LINAC”, MOP194, Proceedings of 2011 PAC, New York, NY, USA

[6] Y. Liu et al., "Laser wire beam profile monitor in the spallation neutron source (SNS) superconducting linac", Nucl. Instr. and Meth. in Phys. Res. section A 612, 241, (2010).

[7] W.B. Cottingame, G.P. Boicourt, J.H. Cortez, W.W. Higgins, O.R. Sander, D.P. Sandoval, "Noninterceptive techniques for the measurement of longitudinal parameters for thr intense H^- beams" IEEE Trans. Nucl. Sci., NS-32(5):1871-1873, 1985.

[8] Datasheet, "20/130 Passive LMA Double Clad Fiber", www.nufern.com

[9] G. Mann et al., "Nanosecond laser damage resistance of differently prepared semi-finished parts of optical multimode fibers", Applied Surface Science 254, pp.1096-1100 (2007)

[10] Rainer Engelbrecht, "Nichtlineare Faseroptik - Grundlagen und Anwendungsbeispiele", Springer, 2014

[11] Coastal Connections, www.coastalconnections.biz, California, USA

[12] CIVIDEC Instrumentation GmbH, www.cividec.at, Austria

ISBN 978-3-95450-176-2